025921-24-T

Ames
Grant

IN-61-CR

69272

P 23

Application of Edge-Based Finite Elements and Vector ABCs in 3D Scattering

A. Chatterjee, J. M. Jin and J. L. Volakis

NAG-2-541

January 1992

THE UNIVERSITY OF MICHIGAN

Radiation Laboratory
Department of Electrical Engineering
    and Computer Science
Ann Arbor, Michigan 48109-2122
USA

Application of Edge-Based Finite Elements and Vector ABCs in 3D Scattering

A. Chatterjee, J. M. Jin and J. L. Volakis

National Aeronautics and
Space Administration
Ames Research Center
Moffett Field CA 94035

Pacific Missile
Test Center
Pt. Mugu CA
03042-5000

January 1992

TECHNICAL REPORT

for NASA Grant NAG-2-541

NASA Technical Monitor: Alex Woo

APPLICATION OF EDGE-BASED FINITE ELEMENTS AND VECTOR ABCS IN 3-D SCATTERING

A. Chatterjee, J.M. Jin and J.L. Volakis
Radiation Laboratory
Department of Electrical Engineering
and Computer Science
University of Michigan
Ann Arbor, MI 48109-2122

Table of Contents

Figures follow page 10

1 Introduction

Open region scattering problems are frequently modelled using an integral
equation formulation[1] and solved using the method of moments. For an
inhomogeneous dielectric scatterer, the integral equation must be discretized
over the entire volume of the object. Since this leads to a full matrix system,
the integral equation technique proves to be expensive in terms of storage
and solution time. Differential equation methods, such as finite elements,
have therefore been tried as an alternative solution approach. Although
these techniques give rise to matrix systems that are considerably larger than
those generated using the integral equation formulation, the finite element
matrices are highly sparse leading to smaller storage and lower solution time.
These methods, however, can only solve bounded field problems whereas
most electromagnetic problems are open boundary-infinite domain types. To
solve for unbounded field problems, the finite element mesh needs to be
truncated artificially at some distance from the scatterer. A wide variety of
methods like ballooning, harmonic series expansions and infinitesimal scaling
have been developed to accomplish this. However, all of the above methods
are 'global' techniques which produce fully populated submatrices that are
computationally expensive and spoil the sparse, banded structure of the finite
element system.

The most promising method of mesh termination developed so far has
been the application of an absorbing boundary condition (ABC) on an artifi-
cial outer boundary to minimise the non-physical reflections from the bound-
ary. The essence of the method is to force the field components at the mesh
termination plane to satisfy the differential equation (absorbing boundary
condition) for an outward travelling wave. The degree of accuracy of the fi-
nite approximation to the differential equation determines the quality of the
mesh termination. Stability considerations limit the degree of approxima-
tion. The advantage of the ABCs over global methods is that they are local
boundary conditions and hence retain the sparse structure of the finite ele-
ment formulation. Moreover, the additional computational effort when using
ABCs is small when compared to a bounded field problem. One disadvan-
tage, however, is that ABCs are approximate and do not model the exterior
field exactly. The local boundary conditions should also give rise to inac-
curacies when travelling waves are excited on the scatterer and substantial
global coupling exists between widely separated parts of the scatterer.

In this report, we consider a FE-ABC solution of the scattering by arbi-
trary three-dimensional structures. The computational domain is discretized
using edge-based tetrahedral elements. In contrast to the node-based ele-
ments, edge elements can treat geometries with sharp edges, are divergence-
less and easily satisfy the field continuity condition across dielectric interfaces
[1]. They do, however, lead to a higher unknown count but this is balanced
by the greater sparsity of the resulting finite element matrix. Thus the com-
putation time required to solve such a system iteratively with a given degree
of accuracy is less than the traditional node-based approach [2].

The purpose of this report is to examine the derivation and performance of the ABCs when applied to two and three dimensional problems and to discuss the specifics of our FE-ABC implementation. The two dimensional ones investigated here are the well-known Bayliss-Turkel[3] and Engquist-Majda[4] absorbing boundary conditions. The three dimensional ABCs presented here are those derived by Mittra[5] and Kanellopoulos and Webb[6]. All the ABCs discussed here are derived from the Wilcox expansion and can only be applied on a spherical outer boundary. Some results are then presented which demonstrate that remarkably accurate solutions can be obtained by enforcing the ABC a small fraction of a wavelength from the scatterer. This is in contrast to our experience with two-dimensional applications and is probably due to the faster ($1/r$ rather than $1/\sqrt{r}$) decay of the propagating fields.

2   Derivation of the ABCs

2.1   Two-dimensional ABCs

Absorbing boundary conditions for two-dimensional problems have been extensively studied over the years. The most notable ABC to come out of this research has been the one proposed by Bayliss, Gunzburger and Turkel[3] who employed an asymptotic analysis to derive a series of local operators. Using the pseudo-differential operator theory, Engquist and Majda[4] have generated a set of different operators for minimisation of the reflections from the mesh termination boundary. However, since the Engquist-Majda ABCs are not as accurate as the Bayliss-Gunzburger-Turkel(BGT) ABCs, only the BGT operators will be discussed here.

Consider a perfectly conducting cylindrical scatterer, shown in Figure 1, whose cross-section is defined by the contour Γ_1. Let the exterior region of the scatterer lie in the domain Ω. For a TM-polarized incident wave, we need to solve the wave equation

$$\nabla^2 u + k^2 u \;=\; 0 \tag{1}$$

in Ω. The wave function u is proportional to the z-component of the scattered electric field and satisfies the boundary condition

$$u^i + u \;=\; 0 \quad \text{on } \Gamma_1 \tag{2}$$

where u^i is the incident wave function.

Following Wilcox, an asymptotic expression for u can be written as follows:

$$
\begin{aligned}
u(\rho,\phi) \;&=\; \frac{e^{-jk\rho}}{\sqrt{\rho}}\left[a_0(\phi) + \frac{a_1(\phi)}{\rho} + \frac{a_2(\phi)}{\rho^2} + \cdots \right] \\
&=\; \frac{e^{-jk\rho}}{\rho^{1/2}} \sum_{n=0}^{\infty} \frac{a_n(\phi)}{\rho^n}
\end{aligned}
\tag{3}
$$

Defining u_ρ as the derivative of u with respect to ρ, we have from (3)

$$u_\rho + jku = -\frac{e^{-jk\rho}}{2\rho^{3/2}}\left[a_0(\phi) + 3\frac{a_1(\phi)}{\rho} + 5\frac{a_2(\phi)}{\rho^2} + \cdots\right] \qquad (4)$$

Therefore, from (4), we obtain

$$u_\rho + jku = O\left[\frac{1}{\rho^{3/2}}\right]$$

Thus if we neglect terms of the order $O(\rho^{-3/2})$ and smaller, we obtain $u_\rho + jku = 0$, which is equivalent to the Sommerfeld radiation condition for the wave function u in two dimensions. It is shown next that a higher-order boundary operator B_1 can be obtained that yield terms of the order $O(\rho^{-5/2})$ when applied to u. The operator B_1 is given by

$$B_1 = \frac{\partial}{\partial\rho} + jk + \frac{1}{2\rho} \qquad (5)$$

It is readily found that, for a given ρ, B_1 introduces a higher order error in ρ^{-1} than does the Sommerfeld radiation condition such that terms of the order $O(\rho^{-5/2})$ and smaller are neglected. Continuing along similar lines, the next higher order operator B_2 can be derived by first defining $v = B_1 u$, and then showing that

$$\left(\frac{\partial}{\partial\rho} + jk + \frac{5}{2\rho}\right)v = O(\rho^{-9/2})$$

The second-order absorbing boundary operator B_2 is thus given by

$$B_2 = \left(\frac{\partial}{\partial\rho} + jk + \frac{5}{2\rho}\right)\left(\frac{\partial}{\partial\rho} + jk + \frac{1}{2\rho}\right) \qquad (6)$$

In fact, it is shown in [3] that a generalised operator B_m can be constructed by repeating the above procedure such that

$$B_m = \prod_{p=1}^{m}\left[\frac{\partial}{\partial\rho} + jk + \frac{2p - 3/2}{\rho}\right] \qquad (7)$$

and

$$B_m u = O\left[\frac{1}{\rho^{2m+1/2}}\right]$$

Since the error between the exact field and the approximated value decreases as we employ higher order boundary conditions, the mesh termination boundary can be brought closer to the scatterer resulting in a smaller number of unknowns. However, the higher order conditions make the system of equations progressively more ill-conditioned and the choice of the order of the

3

ABC is often limited by this constraint. The second order ABC is usually employed in practice.

An alternate derivation[5] of the boundary operators can also be carried out by imposing the requirement that $u(\rho, \phi)$ in (3) satisfy the wave equation and then deriving a recursion relationship in terms of the angular derivatives. The second order ABC thus reduces to

$$
\begin{aligned}
u_\rho &= \left(-jk - \frac{1}{2\rho} + \frac{1}{8jk\rho^2} + \frac{1}{8k^2\rho^3}\right) u + \left(\frac{1}{2jk\rho^2} + \frac{1}{2k^2\rho^3}\right) u_{\phi\phi} + O\left(\frac{1}{\rho^{9/2}}\right) \\
&= \alpha(\rho)u + \beta(\rho)u_{\phi\phi}
\end{aligned}
\tag{8}
$$

Higher order boundary operators in the above formulation involve higher order angular derivatives and are thus simple to implement numerically.

2.2 Three dimensional ABCs

Three dimensional absorbing boundary conditions can be classified into two categories: scalar ABCs and vector ABCs. Most of these boundary conditions are untested till date; it is, therefore, difficult to comment on the performance of these boundary operators. However, in tests carried out using the vector ABC derived in [6], reliable results have been obtained on placing the mesh truncation boundary a fraction of a wavelength distant from the scatterer.

The first section presents a scalar ABC proposed in [5] and the second section is devoted to the formulation of vector ABCs derived in [5] and [6].

2.2.1 Scalar ABC

Let $u(r, \theta, \phi)$ satisfy the scalar wave equation (1) and be expressed asymptotically as

$$
u = \frac{e^{-jkr}}{r} \sum_{n=0}^{\infty} \frac{a_n(\theta, \phi)}{r^n}
\tag{9}
$$

It can then be shown that the coefficients in the series expansion, a_n, satisfy the following recursion relationship

$$
-2jkna_n = n(n-1)a_{n-1} + Da_{n-1}
\tag{10}
$$

where D is Beltrami's operator and is given by

$$
D = \frac{1}{\sin\theta}\frac{\partial}{\partial\theta}\left(\sin\theta\frac{\partial}{\partial\theta}\right) + \frac{1}{\sin^2\theta}\frac{\partial^2}{\partial\phi^2}
\tag{11}
$$

Differentiating (9) with respect to r and incorporating the the recursion relationship repeatedly in the resulting expression yields

$$
u_r = -jk\left\{\alpha(r)u + \beta(r)Du\right\}
\tag{12}
$$

up to and including terms of order r^{-4}. In (12),

$$
\alpha(r) = \left(1 + \frac{1}{jkr}\right) \qquad \beta(r) = \frac{1}{2(kr)^2\alpha(r)}
$$

4

2.2.2 Vector ABC

As for the scalar case, we begin with the Wilcox representation of the electric field which has an expansion of

$$\mathbf{E}(\mathbf{r}) \;=\; \frac{e^{-jkr}}{r} \sum_{n=0}^{\infty} \frac{\mathbf{A}_n(\theta,\phi)}{r^n} \tag{13}$$

where r, θ, ϕ are spherical coordinates. From (13), we get

$$\nabla \times \mathbf{E} = \left\{ -\left(jk + \frac{1}{r}\right)\hat{\mathbf{r}} \times + \frac{D_1}{r}\right\}\mathbf{E} - \frac{e^{-jkr}}{r^2}\sum_{n=1}^{\infty}\frac{n\mathbf{A}_{nt}}{r^n} \tag{14}$$

where $\mathbf{A}_{nt} = \hat{\mathbf{r}} \times \mathbf{A}_n$ is the transverse component of $\mathbf{A}_n$ and, for a vector $\mathbf{F}$, $D_1\mathbf{F}$ is given by

$$\begin{aligned}
D_1\mathbf{F} \;=\; & \frac{1}{sin\theta}\left[\frac{\partial}{\partial\theta}(sin\theta F^\phi) - \frac{\partial F^\theta}{\partial\phi}\right]\hat{\mathbf{r}} \\
& + \frac{1}{sin\theta}\left[\frac{\partial F^r}{\partial\theta} - sin\theta F^\phi\right]\hat{\theta} + \left[F^\theta - \frac{\partial F^r}{\partial\theta}\right]\hat{\phi}
\end{aligned} \tag{15}$$

Using the recursion relation

$$-2jkn\mathbf{A}_{nt} \;=\; n(n-1)\mathbf{A}_{n-1,t} + D_4\mathbf{A}_{n-1}$$

where

$$\begin{aligned}
D_4\mathbf{A}_n \;=\; & \left(D\,A_n^\theta + D_\theta\,\mathbf{A}_n\right)\hat{\theta} + \left(D\,A_n^\phi + D_\phi\,\mathbf{A}_n\right)\hat{\phi} \\
D_\theta\,\mathbf{A}_n \;=\; & 2\frac{\partial A_n^r}{\partial\theta} - \frac{1}{sin^2\theta}A_n^\theta - \frac{2cos\theta}{sin^2\theta}\frac{\partial A_n^\phi}{\partial\theta} \\
D_\phi\,\mathbf{A}_n \;=\; & \frac{2}{sin\theta}\frac{\partial A_n^r}{\partial\phi} - \frac{1}{sin^2\theta}A_n^\phi + \frac{2cos\theta}{sin^2\theta}\frac{\partial A_n^\theta}{\partial\phi}
\end{aligned}$$

and D is Beltrami's operator defined in (11), we can derive the representation correct to r^{-4}. Applying the recursion relation in (14) yields the desired relationship for the vector ABC:

$$\nabla \times \mathbf{E} \;=\; \alpha(r)\mathbf{E} + \beta(r)D_4\mathbf{E} \tag{16}$$

where

$$\begin{aligned}
\alpha(r) \;=\; & jk\left\{\frac{D_1}{jkr} - \left(1 + \frac{1}{jkr}\right)\hat{\mathbf{r}}\times\right\} \\
\beta(r) \;=\; & \frac{1}{2jkr^2}\frac{1}{(1 - 1/jkr)}
\end{aligned}$$

An alternate derivation of the three-dimensional vector ABC is given in [6] which has a higher order of accuracy and is easier to implement than the

previous one. The basic building block is the differential operator L_N, defined as

$$L_N(\mathbf{u}) = \hat{\mathbf{r}} \times \nabla \times \mathbf{u} - \left(jk + \frac{N}{r}\right)\mathbf{u}, \quad N = 0, 1, 2, \ldots \quad (17)$$

where $\hat{\mathbf{r}}$ is a unit vector in the radial direction. It can be shown that for $N \geq 0$ and $n \geq 0$,

$$L_N\left(g\frac{\mathbf{A}_{nt}(\theta, \phi)}{r^{n+1}}\right) = (n - N)g\frac{\mathbf{A}_{nt}(\theta, \phi)}{r^{n+2}} \quad (18)$$

$$L_N\left(\nabla_t\left\{g\frac{A_{nr}(\theta, \phi)}{r^{n+1}}\right\}\right) = (n + 1 - N)\nabla_t\left\{g\frac{A_{nr}(\theta, \phi)}{r^{n+2}}\right\} \quad (19)$$

where g is e^{-jkr} and the subscripts t and r denote the transverse and radial components of a vector, respectively. In both cases, L_N has the effect of multiplying by $1/r$ while leaving the transverse dependence unchanged.

The operators B_N, $N = 1, 2, \ldots$ can now be defined such that

$$B_N(\mathbf{E}) \doteq O\left(\frac{1}{r^{2N+1}}\right)$$

where

$$B_N\left(g\frac{\mathbf{A}_n(\theta, \phi)}{r^{n+1}}\right) = (n + 1 - N)(n + 2 - N)\cdots(n)g\frac{\mathbf{A}_{nt}(\theta, \phi)}{r^{n+1+N}}$$
$$+ s(n + 1 - N)(n + 2 - N)\cdots(n - 1)\nabla_t\left\{g\frac{A_{nr}(\theta, \phi)}{r^{n+N}}\right\}$$
$$(20)$$

Since A_{0r} is zero, it can be seen that the RHS of (20) vanishes for $n = 0, 1, \ldots, N - 1$, i.e., B_N annihilates the first N terms of the vector expansion (13). Thus, $B_N = 0$ is an approximate absorbing boundary condition on the surface S of a sphere of radius r. After a certain amount of algebra and making use of the fact that $\mathbf{E}$ satisfies the vector wave equation, the operators B_1 and B_2 can be written as

$$B_1(\mathbf{E}) = \hat{\mathbf{r}} \times \nabla \times \mathbf{E} - \alpha\mathbf{E}_t + (s - 1)\nabla_t E_r \quad (21)$$

$$B_2(\mathbf{E}) = \frac{1}{\beta}(\hat{\mathbf{r}} \times \nabla \times \mathbf{E}) + \frac{\alpha}{\beta}\mathbf{E}_t + \nabla \times [\hat{\mathbf{r}}(\nabla \times E_r)]$$
$$+ (s - 1)\nabla_t(\nabla \cdot \mathbf{E}_t) + (2 - s)\alpha\nabla_t E_r \quad (22)$$

where $\alpha = jk$ and $\beta = 1/(2jk + 2/r)$. The operator B_2 can be incorporated into a weighted residual formulation for $s = 1$ but leads to an unsymmetric matrix problem. However, for $s = 2$, the functional yields a sparse, symmetric matrix. Thus, the second order boundary operator can be expressed as

$$B_2(\mathbf{E}) = -(\hat{\mathbf{r}} \times \nabla \times \mathbf{E}) + P_2(\mathbf{E})$$

6

where

$$P_2(\mathbf{E}) = \alpha\mathbf{E}_t + \beta\nabla \times [\hat{\mathbf{r}}(\nabla \times \mathbf{E})_r] + (s-1)\beta\nabla_t(\nabla \cdot \mathbf{E}_t) + (2-s)\alpha\beta\nabla_t E_r \quad (23)$$

which can be easily incorporated into the surface integral of the electric field functional.

3 Formulation

3.1 Two-dimensional case

The scattered field must satisfy the wave equation (1) within the domain of interest. The first step in the finite element formulation is to multiply (1) with a test function v and integrate the product over the entire problem domain. This gives

$$\int_\Omega \left(v\nabla^2 u + k^2 vu\right) dS \;=\; 0 \qquad\qquad (24)$$

where u consists of a set of known basis functions weighted by its corresponding unknown coefficients. The second step involves transferring the derivative from the basis function u to the testing function v via Green's identity as follows

$$\int_\Omega v\nabla^2 u \;=\; -\int_\Omega \nabla u \cdot \nabla v\, dS + \int_{\Gamma_1+\Gamma_2} v\frac{\partial u}{\partial n}dl \qquad\qquad (25)$$

Substituting the above identity into (24), we arrive at the weak form of the Helmholtz equation

$$\int_\Omega \left(\nabla u \cdot \nabla v - k^2 uv\right) dS \;=\; \int_{\Gamma_1+\Gamma_2} v\frac{\partial u}{\partial n}dl \qquad\qquad (26)$$

where Γ_1 and Γ_2 describe the boundary of the solution domain as shown in Figure 1. The absorbing boundary condition for two dimensions is to be applied at the contour boundary (Γ_2) and must be expressed in terms of the normal derivative of the wave function. For a Galerkin formulation of (26), we replace the testing function v with the basis function u.

3.2 Three-dimensional case

For simplicity, we consider the problem of 3-D scattering by a conducting body. To solve this problem using the finite element method, it is necessary to enclose the scatterer within a fictitious surface denoted by S. Since the ABCs are derived only for spherical surfaces, the fictitious outer surface in our case is usually a sphere. The scattered field, denoted by $\mathbf{E}$, satisfies the Helmholtz vector equation interior to S and the absorbing boundary condition at S. The equivalent variational problem for this is given by

$$\delta F(\mathbf{E}) = 0$$

7

where F denotes the functional given by [6]

$$F(\mathbf{E}) = \int_V \left[(\nabla \times \mathbf{E}) \cdot (\nabla \times \mathbf{E}) - k^2 \mathbf{E} \cdot \mathbf{E} \right] dV$$
$$+ \int_S \left[\alpha \mathbf{E}_t^2 + \beta (\nabla \times \mathbf{E})_r^2 - \beta (\nabla \cdot \mathbf{E}_t)^2 \right] dS \qquad (27)$$

in which V denotes the volume enclosed by S. To discretize this functional, the volume V is subdivided into a number of small tetrahedra, each occupying the volume V_e ($e = 1, 2, \cdots, M$), where M denotes the total number of elements. Within each element, the electric field is expressed as

$$\mathbf{E}^e = \sum_{j=1}^m E_j^e \mathbf{W}_j^e = \{\mathbf{W}^e\}^T \{E^e\} = \{E^e\}^T \{\mathbf{W}^e\} \qquad (28)$$

where $\mathbf{W}_j^e$ are the edge-based vector basis functions given in [2], E_j^e denote the expansion coefficients of the basis, m represents the number of edges in the element and the superscript stands for the element number. On substituting (28) into (27), we obtain

$$F = \sum_{e=1}^M \{E^e\}^T [A^e] \{E^e\} + \sum_{s=1}^{M_s} \{E^s\}^T [B^s] \{E^s\} \qquad (29)$$

where M_s denotes the number of triangular surface elements on S. Also, the elements of the matrices $[A^e]$ and $[B^s]$ are given by

$$A_{ij}^e = \int_{V_e} \left[(\nabla \times \mathbf{W}_i^e) \cdot (\nabla \times \mathbf{W}_j^e) - k_o^2 \mathbf{W}_i^e \cdot \mathbf{W}_j^e \right] dV$$

$$B_{ij}^s = \int_{S_s} \left[\alpha \mathbf{W}_{it}^s \cdot \mathbf{W}_{jt}^s + \beta (\nabla \times \mathbf{W}_i^s)_r \cdot (\nabla \times \mathbf{W}_j^s)_r - \beta (\nabla \cdot \mathbf{W}_{it}^s)(\nabla \cdot \mathbf{W}_{jt}^s) \right] dS$$

where V_e denotes the volume of the eth tetrahedron and S_s denotes the surface area of the sth triangular surface element on S. On assembling all M elements, (29) can also be written as

$$F = \{E\}^T [K] \{E\}$$

where $[K]$ is a $N \times N$ sparse, symmetric matrix with N being the total number of edges in the geometry and $\{E\}$ is a $N \times 1$ column vector denoting the edge fields. The system of equations is then obtained by applying the Rayleigh-Ritz procedure which amounts to differentiating F with respect to each edge field and then setting the differential to zero. This yields

$$[K]\{E\} = \{0\} \qquad (30)$$

Upon imposing the boundary condition at the surface of the scatterer which states that the total tangential electric field vanishes at the conducting surface, we obtain the final system whose solution yields the field components over the entire domain. In our implementation, only the non-zero elements of the $[K]$ matrix were stored and the resultant system was solved using the biconjugate gradient algorithm.

8

4 Results

Finite element codes have been extensively tested using two-dimensional absorbing boundary conditions and have been known to perform quite well for circular mesh termination boundaries. In figure 2(a), we consider a cylindrical problem[7] to compare the BGT and Engquist-Majda ABCs. This problem is interesting since strong resonant phenomena are observed for small bodies. It consists of a conducting cylinder with a radius of one free-space wavelength covered by a half free-space wavelength thick dielectric with a relative permittivity of 2 and a relative permeability of 2. Figure 2(b) shows the comparison of the bistatic pattern ($\theta_{inc} = 180^\circ$) of two solutions of the BGT ABCs, with the outer boundary at a distance of 1.5λ and $.5\lambda$ away from the scatterer. As expected, the 1.5λ distant boundary produces better results than the $.5\lambda$ distant one. Figure 2(c) plots the performance of the Engquist-Majda ABCs for the same geometry and angle of incidence. The BGT ABC with its outer boundary a mere $.5\lambda$ away outperforms the Engquist-Majda ABC when its outer boundary is 2.5λ distant from the scatterer.

Figure 3(a) analyses two conducting wedges, $5\lambda_o$ long, with the area between them filled with a dielectric having $\epsilon_r = 2$ and $\mu_r = 2$. The incident angle of the incoming plane wave is 0°. Again, the results obtained using the BGT absorbing boundary condition in figure 3(b) matches the data obtained from a hybrid finite element / boundary element analysis. Figure 3(c) shows the corresponding results obtained with the Engquist-Majda ABCs.

In figure 4, we present the backscatter data from a $0.3\lambda \times 0.3\lambda$ plate. The Sommerfeld radiation condition was employed at the mesh termination boundary placed 0.3λ away from the edge. The comparison with a standard integral equation code is seen to be excellent. The backscatter pattern of the same plate is shown in figure 5 with a conformal outer boundary. The zero thickness plate lying at $z = 0$ on the $x - y$ plane was enclosed within a boundary resembling a cut-off sphere. This was achieved by making a plane cut at $z = \pm.3\lambda$ of a $.45\lambda$ radius sphere and setting r in (23) to ∞ over the planar surfaces. Storage was reduced by about 10% on using the conformal outer boundary but the reduction should be more striking for larger geometries.

Figure 6 compares the measured bistatic cross-section ($\theta_i = 180^\circ, \phi_i = 90^\circ$) of a metallic cube having an edge length of 0.755λ with the corresponding pattern computed by the three-dimensional FE-ABC code. The second-order vector ABC was employed at the mesh truncation boundary which was placed only 0.1λ from the edge of the cube. About 33000 unknowns were used for the discretization of the computational domain and the $[A]$ matrix contained a total of 264000 distinct non-zero entries. The storage requirement of this matrix is consequently much smaller than the 2000 unknown system generated by the boundary integral approach which has 4 million non-zero entries.

Figure 7 presents backscatter data for a cylinder of radius 0.3λ and height 0.6λ. The data from the three-dimensional finite element code again compare

9

well with that obtained from a moment method-body of revolution code. The mesh was terminated at a distance of 0.3λ from the edge of the scatterer and the system consisted of about 33000 unknowns and converged to the solution in about 350 iterations when using the Sommerfeld radiation condition. Each iteration took approximately 0.3 seconds on a Cray YMP and on the average it was found that for $N > 25000$, the number of iterations required was of the order of $N/100$.

Figure 8 shows the backscatter pattern on enclosing the pec cylinder in figure 7 with a conformal cylindrical boundary capped at the ends by a spherical surface. The storage was reduced by about 20% but the computed values are off by about 1dB for most incidence angles. The poor results are probably due to the fact that the ABCs were derived only for spherical surfaces and therefore fail on cylindrical boundaries.

The above results point out that the mesh truncation boundary could be placed a few tenths of a wavelength away from the scatterer to obtain reliable results. This is probably because in three dimensions, the scattered fields decrease as $1/r$ whereas in two dimensions, the rate of decrease is proportional to $1/\sqrt{r}$.

5   References

1. A. Bossavit, "A rationale for 'edge-elements' in 3-D fields computations", *IEEE Trans. Magn.*, vol. 24, no. 1, pp. 74-9, Jan. 1988.

2. M.L. Barton and Z.J. Cendes, "New vector finite elements for three-dimensional magnetic field computation", *J. Appl. Phys.*, vol. 61, no. 8, pp. 3919-21, April 1987.

3. A. Bayliss, M. Gunzburger and E. Turkel, "Boundary conditions for the numerical solutions of elliptic equations in exterior regions", *SIAM J. Appl. Math.*, vol. 1, no. 3 , pp. 371-85, September 1980.

4. B. Engquist and A. Majda, "Radiation boundary condition for the numerical solution of waves", *Math. Comp.*, vol. 31, no. 139, pp.629-51, July 1977.

5. R. Mittra, O. Ramahi, A. Khebir, R. Gordon and A. Kouki, "A review of absorbing boundary conditions for two and three-dimensional electromagnetic scattering problems" ,*IEEE Trans. on Magnetics*, vol. 25, no. 4, pp. 3034-9, July 1989.

6. J.P. Webb and V.N. Kanellopoulos, "Absorbing boundary conditions for finite element solution of the vector wave equation",*Microwave and Opt. Tech. Letters*, vol. 2, no. 10, pp. 370-2, October 1989.

7. J. D'Angelo and I.D. Mayergoyz, "On the use of local absorbing boundary conditions for RF scattering problems", *IEEE Trans. on Magnetics*, vol. 25, pp. 3040-2, July 1989.
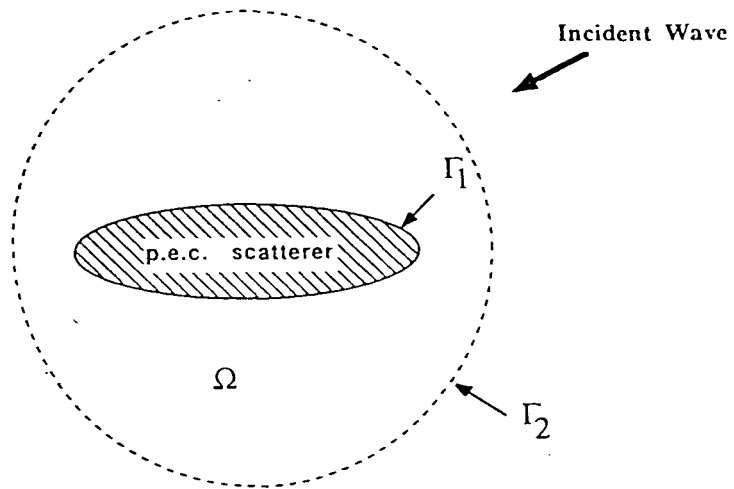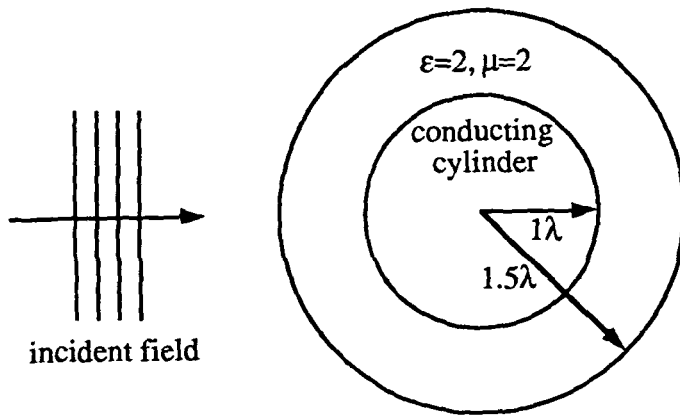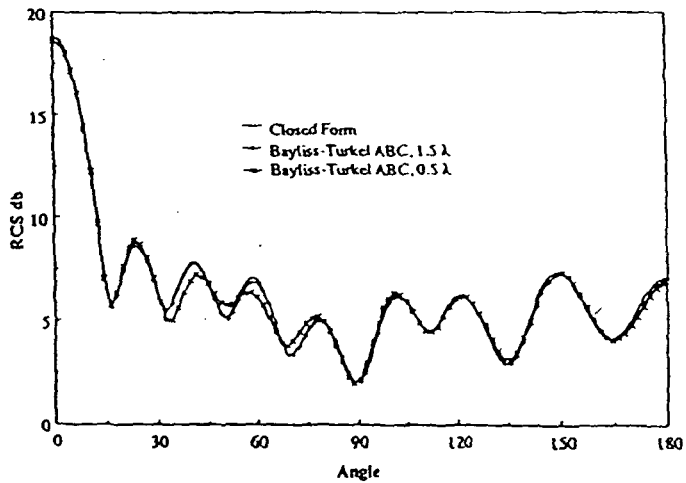
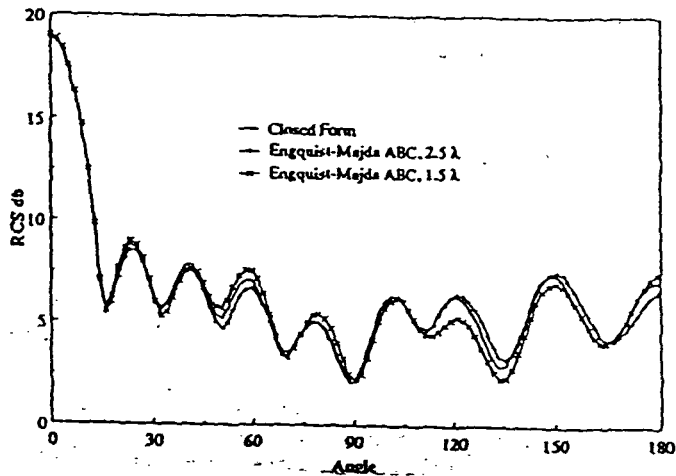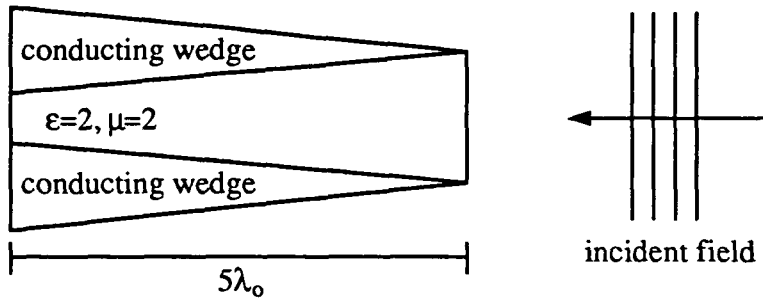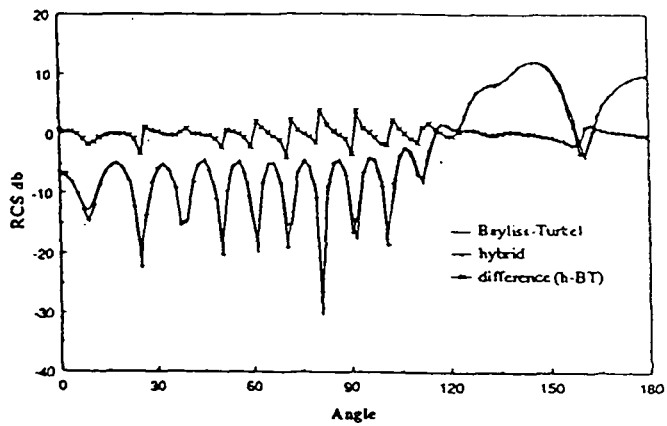Figure 1: Geometry of p.e.c scatterer enclosed in an outer circular boundary
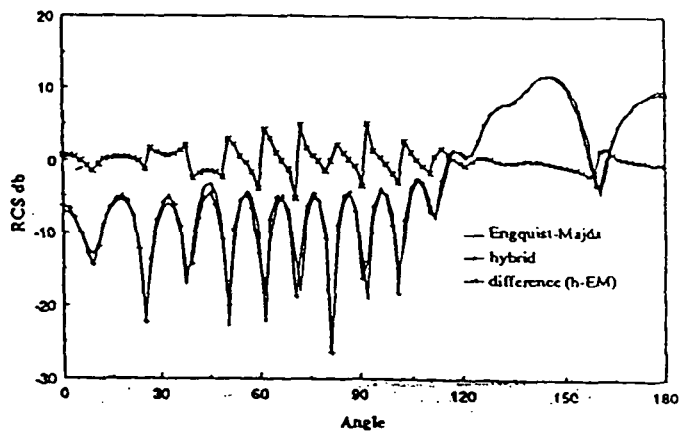
Figure 2: (a)Cylinder geometry (b)Bistatic pattern using BGT absorbing boundary conditions (c)Bistatic pattern using Engquist-Majda absorbing boundary conditions

(a)

(b)

(c)

Figure 3: (a)Wedge geometry (b)Bistatic pattern using BGT absorbing boundary conditions (c)Bistatic pattern using Engquist-Majda absorbing boundary conditions
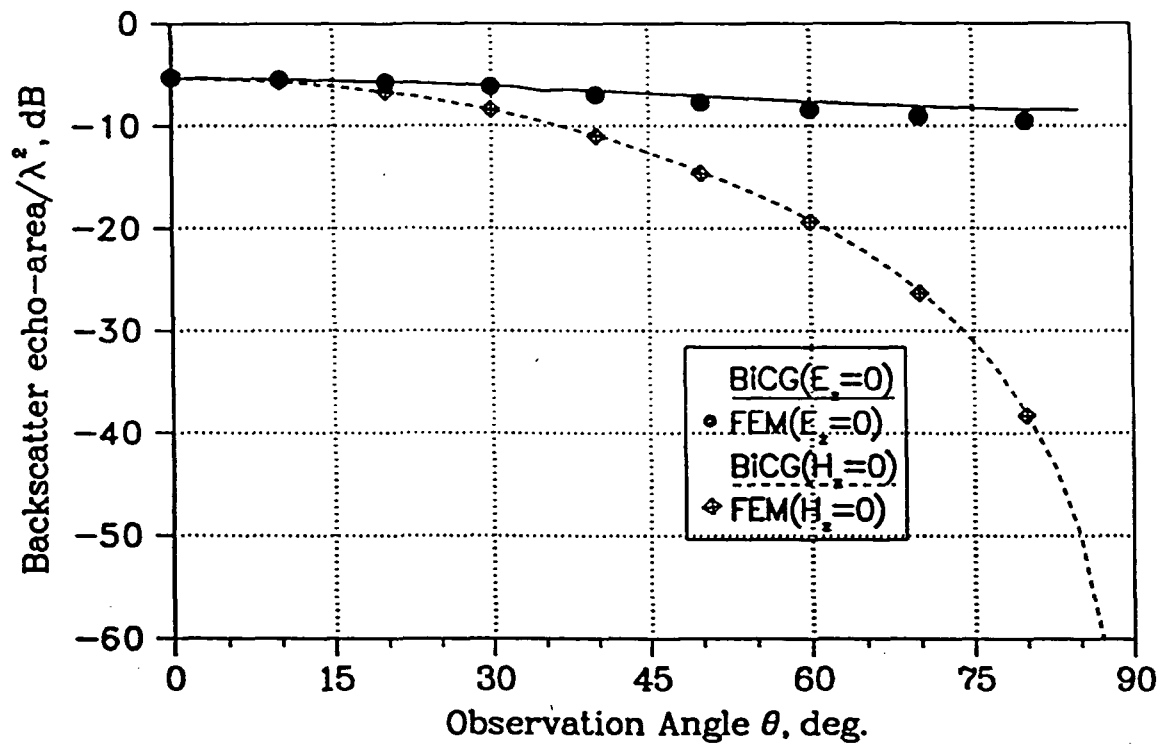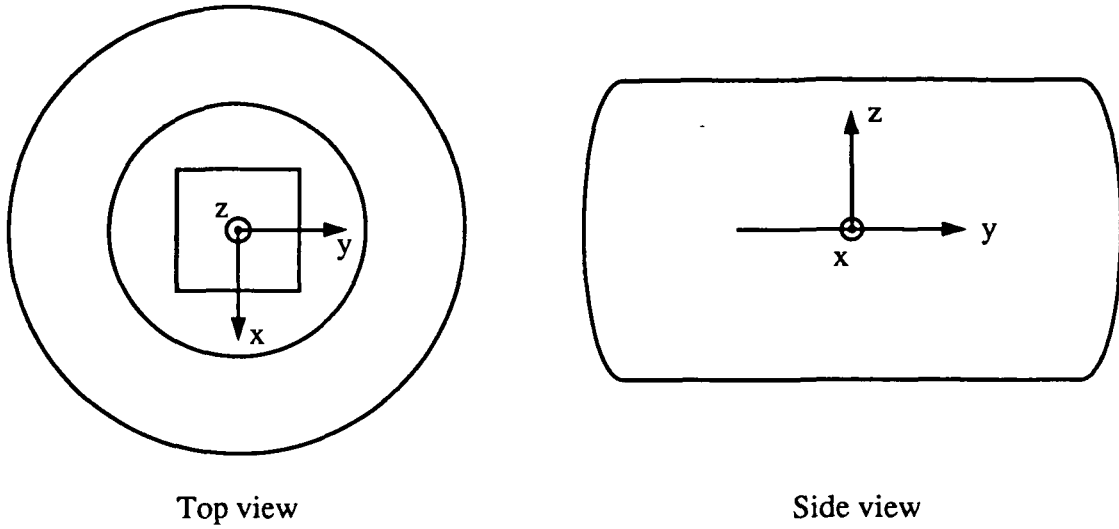
Backscatter pattern of a .3λx.3λ plate

Figure 4: Backscatter pattern of plate using Sommerfeld radiation condition

Top view   Side view

Backscatter pattern of a .3λx.3λ plate

2nd order ABC; cut-off sphere
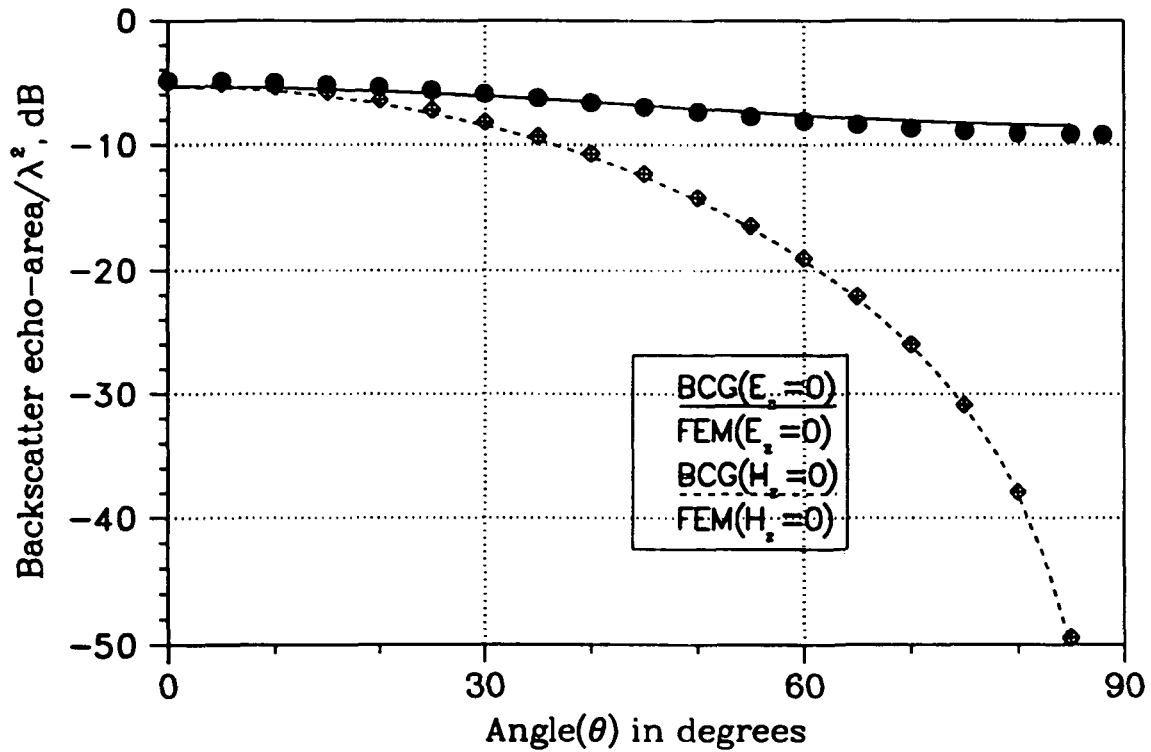
Figure 5: Backscatter pattern of the plate in figure 4 enclosed by a conformal outer boundary and using the 2nd order absorbing boundary condition.
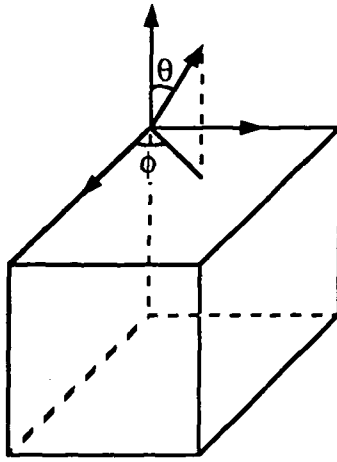
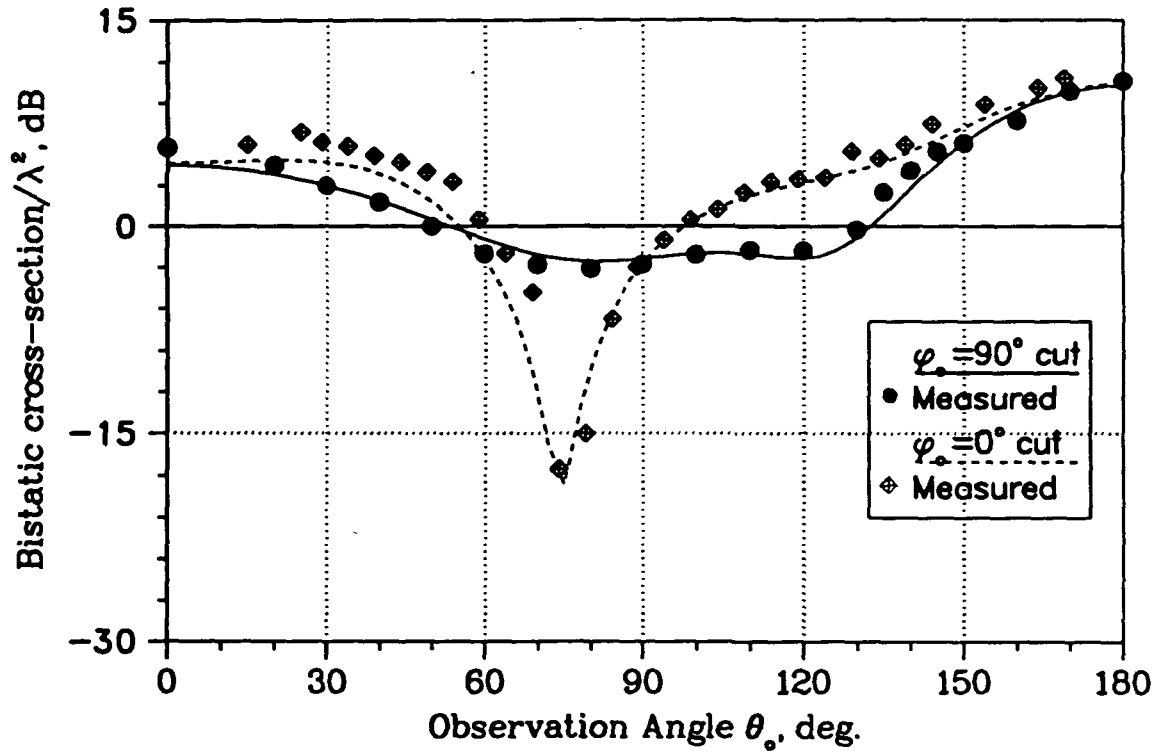# Bistatic pattern of a .755 λ metallic cube

$\theta_i = 180°$

Figure 6: Bistatic pattern ($\theta_i = 180°$) of a metallic cube having an edge length of 0.755λ using the 2nd order vector absorbing boundary condition.

Backscatter pattern of a metallic cylinder

base radius=.3λ   height=.6λ

Backscatter echo-area/λ², dB

Observation Angle θ_o, deg.
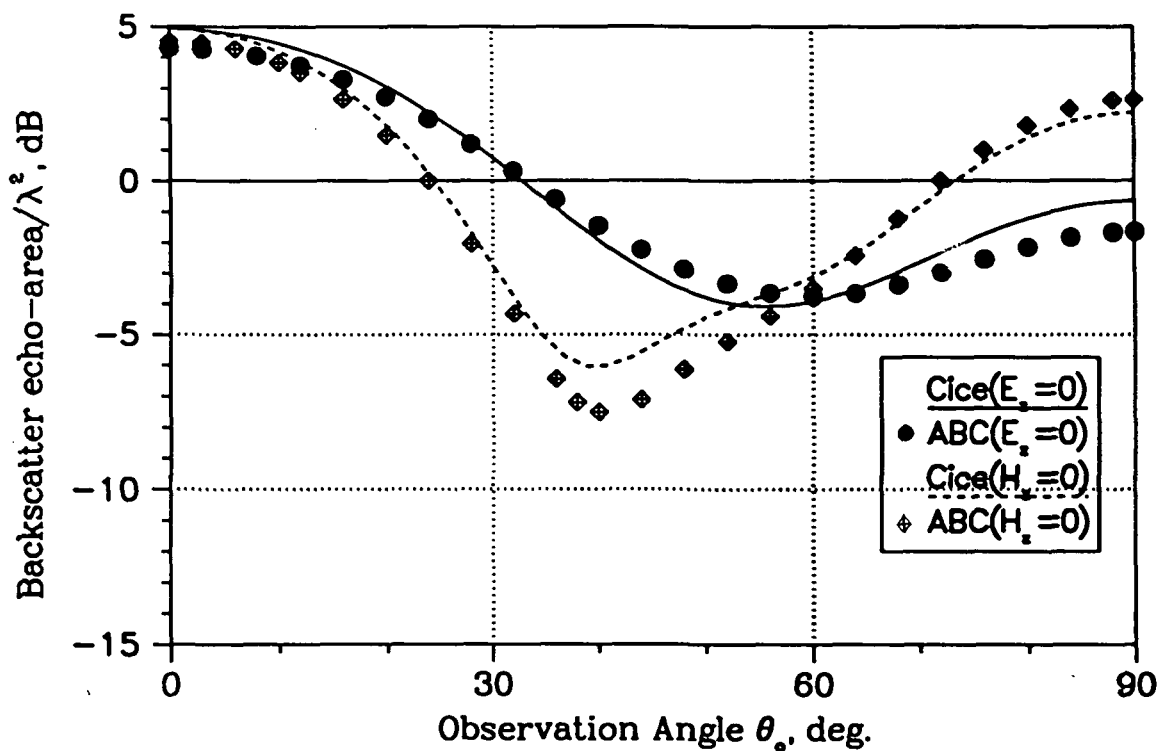
Cice(E_z=0)
• ABC(E_z=0)
Cice(H_z=0)
⟡ ABC(H_z=0)
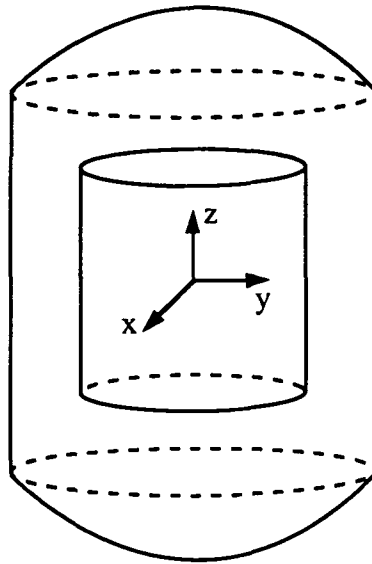
Figure 7: Backscatter pattern of a metallic cylinder of radius 0.3λ and height 0.6λ using the Sommerfeld radiation condition. The axis of the cylinder coincides with the z-axis of the coordinate system.

Backscatter pattern of pec cylinder (r=.3λ,h=.6λ)

2nd order ABC; conformal boundary (20% storage reduction)

Legend:
- Cicero(E_z=0)
- ● FEM(E_z=0)
- Cicero(H_z=0)
- ⊕ FEM(H_z=0)

Y-axis: Backscatter echo-area/λ^2, dB
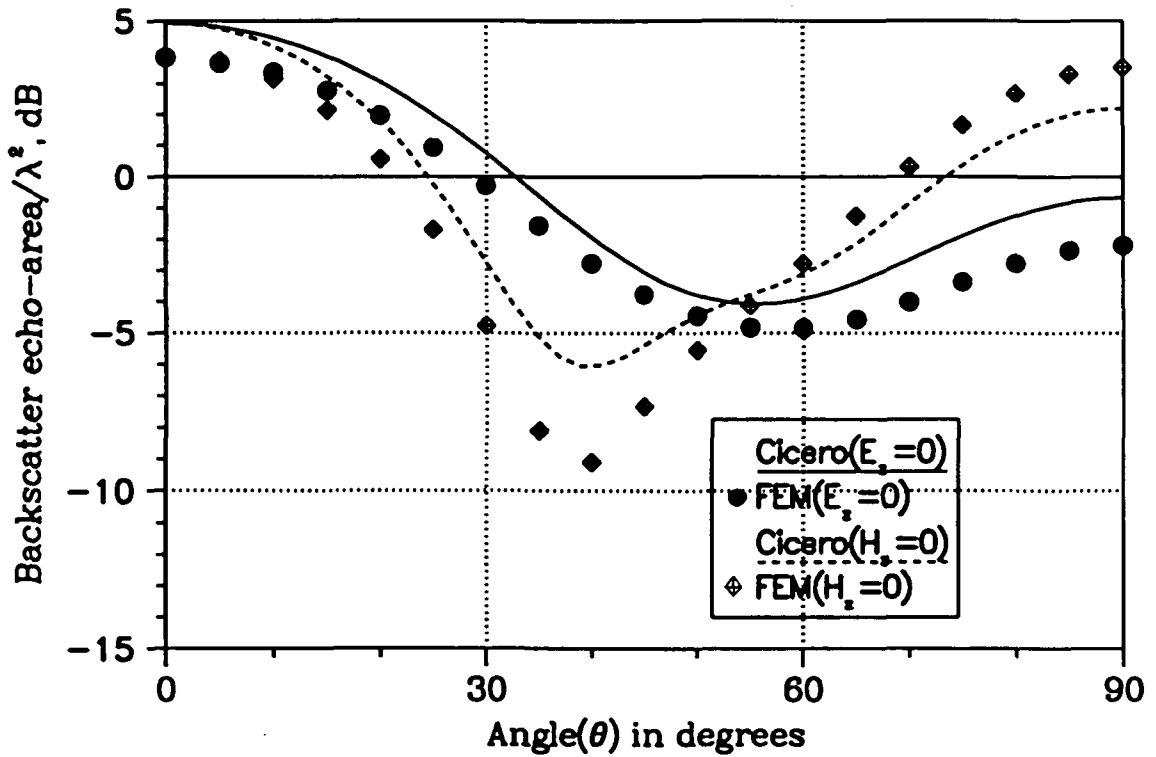X-axis: Angle(θ) in degrees

Figure 8: Backscatter pattern of the cylinder in figure 7 enclosed by a conformal outer boundary and using the second order absorbing boundary condition.